NANO LETTERS

Letter

pubs.acs.org/NanoLett

Strong Coupling between ZnO Excitons and Localized Surface Plasmons of Silver Nanoparticles Studied by STEM-EELS

Jiake Wei,[†,‡] Nan Jiang,[†] Jia Xu,[§] Xuedong Bai,[*,‡,∥] and Jingyue Liu[*,†]

[†]Department of Physics, Arizona State University, Tempe, Arizona 85287, United States

[‡]Beijing National Laboratory for Condensed Matter Physics and Institute of Physics, Chinese Academy of Sciences, Beijing 100190, China

[§]School for Engineering of Matter, Transport and Energy, Arizona State University, Tempe, Arizona 85287, United States

[∥]Collaborative Innovation Center of Quantum Matter, Beijing 100190, China

Supporting Information

ABSTRACT: We investigated the strong coupling between the excitons of ZnO nanowires (NWs) and the localized surface plasmons (LSPs) of individual Ag nanoparticles (NPs) by monochromated electron energy loss spectroscopy (EELS) in an aberration-corrected scanning transmission electron microscopy (STEM) instrument. The EELS results confirmed that the hybridization of the ZnO exciton with the LSPs of the Ag NP created two plexcitons: the lower branch plexcitons (LPs) with a symmetrical dipole distribution and the upper branch plexcitons (UPs) with an antisymmetrical dipole distribution. The spatial maps of the LP and UP excitations reveal the nature of the LSP−exciton interactions. With decreasing size of the Ag NP the peak energies of the LPs and UPs showed a blue-shift and an anticrossing behavior at the ZnO exciton energy was observed. The coupled oscillator model explains the dispersion curve of the plexcitons and a Rabi splitting energy of ∼170 meV was deduced. The high spatial and energy resolution STEM-EELS approach demonstrated in this work is general and can be extended to study the various coupling interactions of a plethora of metal−semiconductor nanocomposite systems.

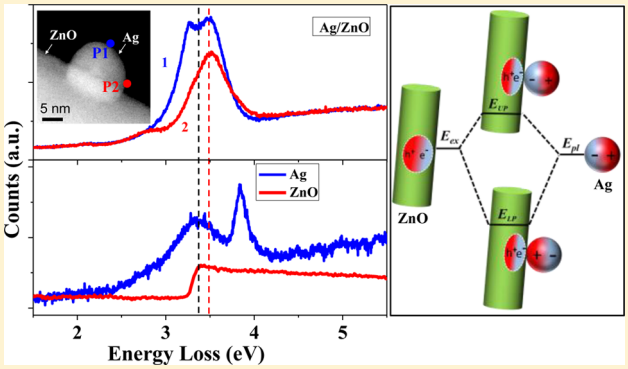

KEYWORDS: *STEM-EELS, plasmonics, excitons, strong coupling, silver nanoparticle, ZnO nanowire*

Nanoscale composites of metallic nanoparticles (NPs) and semiconductor nanostructures provide unique properties and have been intensively investigated.[1−13] The complementary optical properties of the composite heterostructures,[8] the long-lived excitons in semiconductors, and the localized electromagnetic modes in metal NPs make it possible to design specific optical responses and to explore new phenomena as a consequence of exciton−plasmon coupling.[3,14−19] For example, interactions between excitons of a semiconductor nanostructure and the surface plasmons of a metal NP can occur when the semiconductor and metal nanostructures are placed in close proximity such as in a semiconductor−metal nanocomposite. Exciton−plasmon coupling, which originates from the Coulomb interaction between the dipole moments of the excitons and the electromagnetic field of the surface plasmons,[8,9] can be divided into two regimes: (1) weak coupling and (2) strong coupling. In the weak coupling regime, the wave functions of the excitons and plasmons are unperturbed, and the enhanced absorption cross-section,[20,21] increased radiative emissions,[21,22] and exciton−plasmon energy transfers[23,24] have been investigated. The strong coupling occurs when the strength of the plasmon−exciton interaction becomes dominant with respect to the damping dissipation in the system.[8] In this regime, the excitation modes of the plasmonic and excitonic systems are hybridized and such hybridization significantly modifies their dispersion properties, leading to the formation of plexcitons, which possess an anticrossing behavior in their energy dispersion curves and an energy gap defined by the Rabi energy splitting.[6,14,25] The plexcitons possess unique properties different from those of the semiconductor excitons and the metal plasmons. Fundamental understanding of the plexcitons of nanocomposite systems may open new routes to designing novel optical and optoelectronic devices with desirable properties and provide new insights into the understanding of photovoltaic and photocatalytic systems.

Exciton−plasmon coupling in organic and inorganic systems with metallic structures have been intensely studied by optical measurements.[20,25−32] We report here, for the first time, the investigation of the strong coupling between excitons of ZnO nanowires (NWs) and the localized surface plasmons (LSPs) of

Received: May 22, 2015
Revised: July 30, 2015
Published: August 3, 2015

DOI: 10.1021/acs.nanolett.5b02030
Nano Lett. 2015, 15, 5926−5931

individual Ag NPs by ultrahigh energy-resolution electron energy loss spectroscopy (EELS) in a monochromated and aberration-corrected scanning transmission electron microscopy (STEM) instrument. Zinc oxide, which possesses a wide direct band gap (E_g = 3.3 eV at 300 K) and a large exciton binding energy (60 meV), has broad applications in many fields, especially optoelectronic devices or systems.[33−37] The giant enhancement of light emission in the coupled Ag/ZnO and Au/ZnO nanocomposites has been reported, and the enhancement is attributed to the exciton−plasmon coupling.[38−44] However, most of the coupling examples of metal/ZnO heterostructures, reported in the open literature, suffer from a large energy separation between the energy of the metal surface plasmon and the near-UV band gap of ZnO.[27] Nanostructures of Ag, with its low intrinsic losses, narrow surface plasmon resonances, high oscillator strengths, and large optical field enhancements are ideal for studying the surface plasmon related phenomena. Recent experiments demonstrated that, when the size of an Ag NP decreases to nanometer scale, the energy of their LSPs shows a blue-shift toward the UV region.[45,46] Therefore, we hypothesized that, by decreasing the size of the Ag NPs, we can tune the energy of the Ag LSPs to closely match the energy of the ZnO excitons, and consequently strong coupling between the ZnO excitons and the LSPs of the Ag NPs should occur provided that the Ag NP is located in close proximity to a ZnO nanostructure.

With the ultrahigh energy resolution achievable (~9 meV) in a new monochromated and aberration-corrected STEM instrument (Nion UltraSTEM100MC-HERMES),[47] we observed the formation of two new plexcitons (labeled as lower branch plexciton (LP) and upper branch plexciton (UP)) as a result of strong coupling between a ZnO NW and an Ag NP which was attached to the ZnO NW. By using the spectrum imaging technique, spatial distributions of the new excitation modes can be readily obtained.[48] We found that by tuning the size of the Ag NPs from ~40 nm to ~4 nm in diameter, a significant blue-shift of both the LP and UP with an anticrossing behavior at the ZnO exciton energy was observed. The size-dependent behavior of the plexcitons originates from the size dependence of the energy of the Ag LSPs. By invoking a simple coupled oscillator model to describe the plexcitons and fitting the calculations to experimental data, the coupling strength was estimated, and a Rabi splitting of ~170 meV was obtained.

Figure 1a shows a low-magnification high-angle annular dark-field (HAADF) STEM image of the Ag/ZnO NW nanocomposite system, clearly revealing the spatial configurations of the deposited Ag NPs and the ZnO NWs. Figure S1 shows a schematic diagram illustrating the synthesis processes of the Ag/ZnO nanocomposites and Figure S2 shows more HAADF-STEM images of the Ag NPs attached to the ZnO NWs. Detailed descriptions of the sample preparation methods are described in the Supporting Information. Figure 1b displays the EELS spectra acquired at two different locations from the Ag/ZnO NW shown in Figure 1c: At the outer edge of the Ag NP (P1 position) and near the interface between the Ag NP and the ZnO NW (P2 position). The size of the Ag NP is approximately 14 nm in diameter. Two main peaks, at 3.26 and 3.49 eV, can be identified. On the other hand, the EELS spectrum obtained from the isolated Ag NP with a similar size reveals a broad surface plasmon peak around 3.33 eV and a sharp bulk plasmon peak at 3.80 eV (blue curve in Figure 1d). Figure S3 provides more EELS spectra obtained at the different

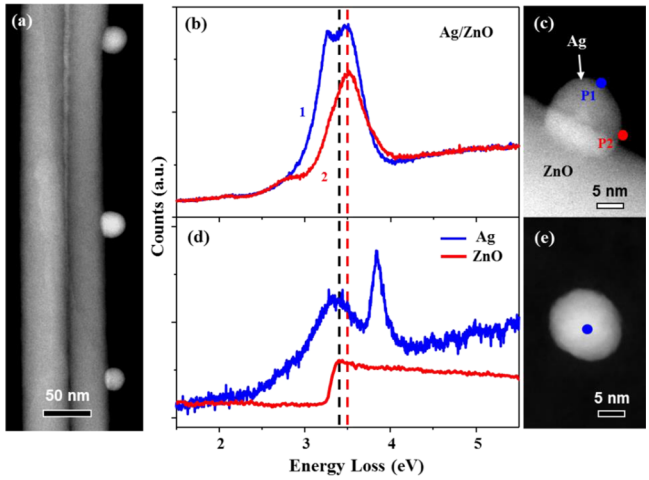

Figure 1. (a) HAADF-STEM image shows the configuration of the Ag/ZnO NW nanocomposite system; (b) EELS spectra of the Ag/ZnO NW obtained from two different positions (P1 and P2 in panel c); (c) HAADF-STEM image of an Ag/ZnO NW with the size of the Ag NP ~ 14 nm; (d) EELS spectra obtained from an isolated Ag NP shown in panel e (blue curve) and from a pure ZnO NW (red curve); and (e) HAADF-STEM image of an isolated Ag NP with a size of ~14 nm. The filled circles in c and e correspond to the positions where the EELS spectra were obtained. The dotted vertical black line indicates the peak position of the ZnO excitons, and the dotted red line indicates the peak position of the upper plexciton.

locations of the isolated Ag NP with a prominent broad surface plasmon peak centered at 3.48 eV. Our results agree with the report that the main surface plasmon mode in the isolated small Ag NPs (<30 nm) is the dipole mode.[45,46,49] Although it has been reported that multipole plasmons can be observed in encapsulated Ag NPs,[50] the high-order surface plasmon modes in small NPs are usually weak and were not detected in our experiments. The blue-shift from 3.33 eV of the 14 nm Ag NP (Figure 1d) to 3.48 eV of the 10 nm Ag NP (Figure S3) clearly manifests the size-dependence of the energy of the Ag LSPs. The blue-shift of the LSP resonance energy with decreasing size of the Ag NPs has been experimentally observed.[45,46] However, the origin of such change of resonance energy with decreasing size is still not completely understood. Furthermore, Figure 1d clearly reveals a relatively sharp bulk plasmon peak and a broad LSP peak of small Ag NPs. Various factors could contribute to the peak broadening: nonspherical geometry, surface electronic states, effect of substrate or surface coatings, quantum confinement, etc. Further defined and systematic research is needed to understand the peak broadening of small metallic NPs.

The EELS spectrum obtained from a pure ZnO NW is displayed in Figure 1d (the red curve) for comparison. Although ZnO is a direct band gap semiconductor, the expected $(E - E_g)^{1/2}$ shape of the band edge[51] was not observed. This is most probably caused by the band gap overlap with the ZnO exciton energy at approximately 3.43 eV.

The two new peaks at 3.26 and 3.49 eV (Figure 1b) observed in the Ag/ZnO composite system must originate from the interaction between the Ag NP and the ZnO NW, a manifestation of strong coupling between the Ag LSPs and the ZnO excitons. The Ag/ZnO NWs were supported by lacey carbon film, and both the Ag NP and the ZnO NW shown in Figure 1c were hanging in vacuum. Therefore, the Ag NP was only in contact with the ZnO NW. The hybridization between

DOI: 10.1021/acs.nanolett.5b02030
Nano Lett. 2015, 15, 5926−5931

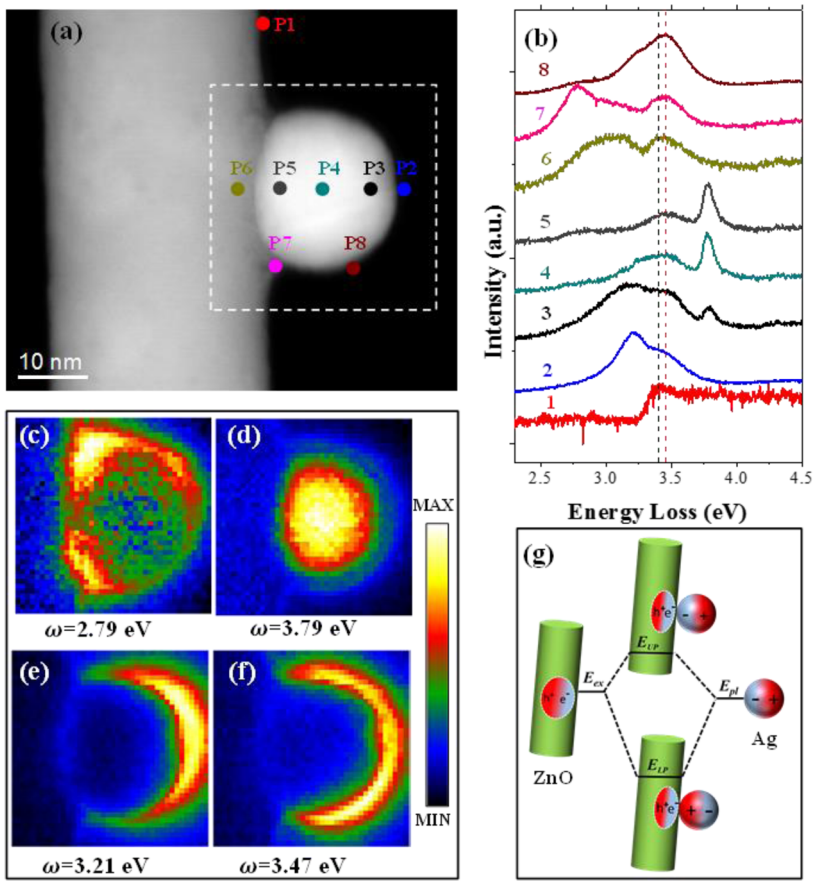

Figure 2. HAADF-STEM image of an Ag/ZnO NW (a) shows the configuration of the Ag NP with respect to the ZnO NW. The filled circles indicate the locations where the corresponding spectra (b) were collected. The EELS maps shown in c, d, e, and f were obtained from the region indicated by the dotted white rectangle in panel a. (b) A series of EELS spectra collected by positioning the electron probe at the various locations shown in a. The dotted vertical black line indicates the peak position of the ZnO exciton and the dotted vertical red line indicates the shifted peak position in the Ag/ZnO system. (c, d, e, f) EELS maps of the peaks at 2.79. 3.79, 3.21, and 3.47 eV, respectively. (g) Schematic drawing of the proposed model of the hybridization of ZnO excitons with the LSPs of the Ag NP.

the Ag LSPs and the ZnO excitons created two new modes, which were defined earlier as UP and LP, respectively. The energies of these two plexcitons can be estimated by a simple coupled oscillator model and are given by[14,16,26,52]

$$E_{\mathrm{UP,LP}} = \frac{1}{2}[E_{\mathrm{ex}} + E_{\mathrm{pl}} \pm \sqrt{4\Omega_0^2 + (E_{\mathrm{ex}} - E_{\mathrm{pl}})^2}\,] \quad (1)$$

in which E_{ex} and E_{pl} are the corresponding energies of the excitons and the LSPs, respectively, and Ω_0 is defined as the coupling energy between the Ag LSPs and the ZnO excitons. We assign the experimentally obtained peak at 3.49 eV to the UP and the peak at 3.26 to the LP, respectively.

Another important feature observed in the Ag/ZnO NW is that the relative intensities of the LP and UP peaks vary with the location of the incident electron probe. As shown in Figure 1b, both peaks have high intensity at the P1 position. But when the electron beam was positioned at the interfacial region of P2, the UP peak is much stronger than the LP peak, suggesting that the excitation of the hybridized LP and UP is spatially distinguishable. The Ag NP shown in Figure 2a is ~20 nm in diameter. The spectrum no. 1 shown in Figure 2b was acquired from a position on the ZnO NW with a large distance away from the Ag NP (P1 in Figure 2a) so that the interaction between the Ag NP and the ZnO NW can be negligible. This spectrum shows similar features with those of the bare ZnO (cf. Figure 1c) with the exciton peak at 3.43 eV. Spectra nos. 2−6 were acquired across the Ag NP, from the outer edge (P2) into the ZnO NW (P6), and spectra nos. 7 and 8 were both obtained on the edges of the Ag NP, but the spectrum no. 7 was obtained from a location very close to the Ag/ZnO interface. Although each spectrum is dominated by different peaks, overall four peaks can be identified: 2.79, 3.21, 3.47, and 3.79 eV. The peaks at 3.21 and 3.47 eV correspond to the LP and UP hybridization modes. The peak at 3.79 eV, revealed clearly in the spectra no. 3, 4, and 5, is the bulk plasmon peak of Ag. The 2.79 eV peak reflects the excitation of the interface plasmon of the Ag/ZnO system. When the electron beam was scanned from P2 to P6, the relative intensities of the LP and UP changed; the UP peak decreased slightly, while the LP peak dropped drastically. When the beam was placed near the ZnO NW (P5), the LP peak almost disappeared. However, after the electron beam was positioned on the ZnO NW (P6), both the LP and UP modes were excited again. When the electron beam was scanned along the perimeter of the Ag NP (P2 → P8 → P7), similar variations of the relative intensities of the UP and LP peaks were observed (see spectrum nos. 2, 7, and 8).

Figure 2c−f shows the spatial excitations of the four main peaks discussed above. These maps were obtained by integrating the peak intensity with an energy window of 0.1 eV. Figure 2c−d reveal the excitation of the interface and bulk plasmons, respectively. Figure 2e and f shows, respectively, the spatial excitation of the LP and UP modes. Note that the LP is

DOI: 10.1021/acs.nanolett.5b02030
Nano Lett. 2015, 15, 5926−5931

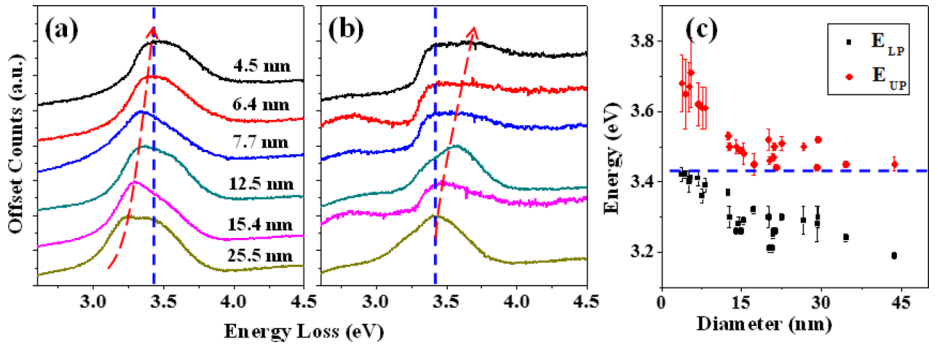

Figure 3. (a) A series of EELS spectra obtained from Ag NPs of various sizes with the electron beam located at the outer edge of the Ag NPs (cf. P2 in Figure 2a). (b) As in panel a, but the EELS spectra were obtained with the electron beam located near the Ag/ZnO interfacial region (cf. P8 in Figure 2a). The dotted red arrows guide the observation of the blue-shift of the energies of the LP and UP modes with decreasing size of the Ag NP. (c) Plots of the energy of the LP and UP mode in the strongly coupled Ag/ZnO NW system as a function of the size of the Ag NPs. The dotted blue lines in a, b, and c indicate the ZnO exciton energy at 3.43 eV.

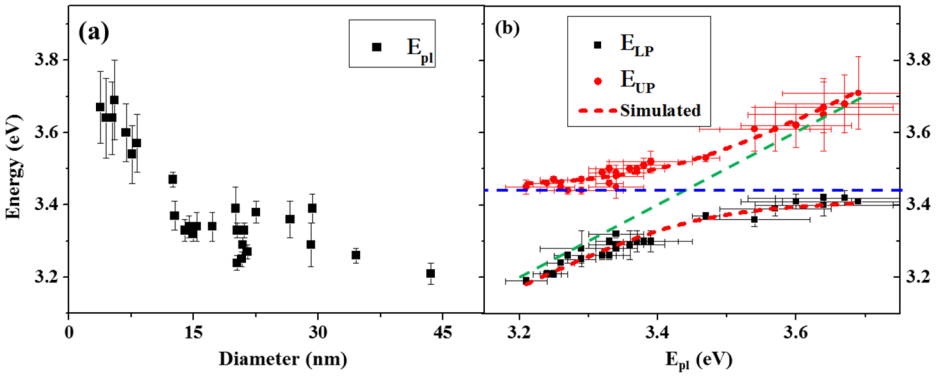

Figure 4. (a) Plot of the LSP resonance energy of isolated individual Ag NPs vs particle size; the energy values were extracted from the EELS data set shown in Figure 3 ($E_{pl} = E_{LP} + E_{UP} - E_{ex}$). (b) Plots of the energies of the LP and UP mode against the corresponding LSP resonance energy of isolated individual Ag NPs of different sizes shown in a. The dotted red lines are the simulated dispersion curves of the UP and LP modes. The dotted blue line indicates the exciton energy of the ZnO NW, and the dotted green line represents the LSP resonance energy of noninteracting individual Ag NPs.

only excited at the outer edge of the Ag NP, while the UP can be uniformly excited on the surfaces of the Ag NP. These excitation maps are similar to those of the symmetric bright and antisymmetric dark mode induced by surface plasmon hybridization of metal dimer NPs.[49,53−55] In our case, the strong coupling is due to the hybridization between the LSPs of the Ag NP and the excitons of the ZnO NW. As schematically illustrated in Figure 2g, the hybridization induced the formation of the two plexcitonic modes: the lower energy LP mode has a symmetrical dipole distribution, while the higher energy UP mode has an antisymmetrical dipole distribution.

Theoretically, when the high-energy fast electrons travel through the Ag/ZnO or in an aloof beam configuration both the LSPs of the Ag NP and the excitons of the ZnO NW are excited, inducing the polarization of both components. The polarized Ag NP and the ZnO NW then interact with each other and the amplitude of the excited LSPs of the Ag NP near the ZnO NW can be deduced by[16]

$$a_p = f(\omega) \oint \tau(\vec{r}_i)\hat{n}_i \cdot [\vec{E}_0(\vec{r}_i) + \vec{E}_x(\vec{r}_i)]\mathrm{d}S_i \qquad (2)$$

in which $\vec{E}_0$ is the electric field produced by the incident electron beam and $\vec{E}_x$ is the electric field induced by the polarized ZnO NW. The parameter $f(\omega)$ is a frequency-dependent factor related to the polarizability of the dipole moment of the Ag NP and τ is surface dipole distribution. The integrals are evaluated on the surface S of the Ag NP and $\hat{n}_i$ is the surface normal at a point $\vec{r}_i$. Strong coupling occurs when the internal electric field is much larger than the external field generated by the incident electron beam.[56] Close to the resonance frequency of the LSP of the Ag NP, the frequency dependent factor $f(\omega)$ in eq 2 can be approximated by[16,57]

$$f(\omega) \approx -\frac{A_p}{(4\pi\epsilon_b)^2(\omega - \omega_{pl})} \qquad (3)$$

in which ϵ_b is the background permittivity, A_p (>0) is a constant that depends on the resonant mode, and ω_{pl} is the resonance frequency of the surface plasmon. At the LP energy level ($\omega < \omega_{pl}$), $f(\omega) > 0$. The LSP excitation of the Ag NP is mainly due to the electric field produced by the ZnO excitons. According to eq 2, for the LP, the surface dipole distribution $\tau(\vec{r})\hat{n}$ on the Ag NP have the same directions with the electric field ($\vec{E}_0\ \vec{r}$), resulting in a symmetrical dipole distribution (Figure 2g). On the other hand, for the UP energy level ($\omega > \omega_{pl}$), $f(\omega) < 0$, the surface dipole distribution $\tau(\vec{r})\hat{n}$ has opposite directions with repect to $\vec{E}_x(\vec{r})$, resulting in an antisymmetrical dipole distribution (Figure 2g). When the electron beam is located at the outer edge of the Ag NP (P1 in Figure 1b and P2 in Figure 2a), both the symmetrical modes (LP) and the asymmetrical modes (UP) can be highly excited. On the other hand, when the electron beam is positioned near the interfacial region

DOI: 10.1021/acs.nanolett.5b02030
Nano Lett. 2015, 15, 5926−5931

between the Ag NP and the ZnO NW, the induced electric fields on the Ag NP and the ZnO NW, parallel to the electron beam traveling direction, are opposite, resulting in cancellation or weak excitation of the symmetrical modes,[49] but the UP mode is still highly excited.

To understand how the energy of the plexcitons can be tuned by the size of the Ag NPs, a series of EELS measurements were performed with the sizes of the Ag NPs varying from ∼40 nm to ∼4 nm in diameter. Figure 3a and b shows the EELS spectra of six individual Ag NPs (with sizes of 25.5, 15.4, 12.5, 7.7, 6.4, and 4.5 nm) attached to individual ZnO NWs when the electron beam was positioned at the P2 (cf. Figure 2a) and P8 (cf. Figure 2a) locations, respectively. As shown in Figure 1, both the UP and LP have higher peak intensity at the outer edge (P1 in Figure 1c) whereas the UP has high peak intensity near ZnO (P2 in Figure 1c) as well. The spectra in Figure 3a (3b) are used to determine the peak positions of LP (UP). A significant blue-shift of both the LP and UP modes were detected when the size of the Ag NP decreased from ∼25 nm to ∼4 nm in diameter. Figure 3c plots such size dependence of the energy of the LP and UP modes for Ag NPs with sizes from ∼40 nm to ∼4 nm. Although many experimental factors influence the accurate determination of the peak energies of the LP and UP excitation modes, the plots in Figure 3c still show significant and systematic blue-shift of both the LP and UP energies when the size of the Ag NP decreases. Such a blue-shift in energy can be understood if we assume that the resonance energies of the LSPs of the Ag NPs depend on their sizes. Therefore, the resonance energies of the LSPs of isolated individual Ag NPs vs particle size can be deduced from eq 2 and the data set in Figure 3c ($E_{pl} = E_{LP} + E_{UP} - E_{ex}$). As shown in Figure 4a, when the size of the Ag NP decreased from ∼40 nm to ∼4 nm in diameter, their LSP resonance energy shifted from ∼3.20 eV to ∼3.70 eV, in agreement with the previously reported EELS measurements of Ag NPs supported on ultrathin substrates.[45,46,58] Since the Ag NPs were attached only to the ZnO NWs and were not supported by any other substrate, the data shown in Figure 4a are free from any substrate effects. The corresponding energy shift of the LP mode in the strongly coupled Ag/ZnO system is limited to a maximum value of 3.43 eV (blue dotted line in Figure 3) and the energy shift of the UP mode is limited to a minimum value of 3.43 eV, clearly demonstrating an anticrossing behavior at the exciton energy (3.43 eV) of the ZnO NW. Figure 4b plots the energies of the LP and the UP modes as a function of the LSP resonance energy of the isolated individual Ag NPs. By fitting these data to eq 1, one can easily extract the interaction energy Ω_0 of our Ag/ZnO nanocomposite system, which is ∼85 meV, resulting a Rabi energy splitting of 170 meV ($2\Omega_0$).

Conclusion. In summary, we have observed strong exciton−plasmon coupling between ZnO NWs and Ag NPs by monochromated STEM-EELS technique. The hybridization of ZnO excitons with LSPs of Ag NPs created two new plexcitons (LP and UP). The spatial maps of the LP and UP excitation modes have been determined and interpreted by the dipole distributions of LP and UP. By tuning the size of the Ag NPs from ∼40 nm to ∼4 nm, an anticrossing behavior has been detected on the Ag/ZnO nanocomposite system; the coupling strength was estimated, and a Rabi energy splitting of ∼170 meV was determined. The high spatial and energy resolution STEM-EELS approach demonstrated in this work is general and can be extended to study many important metal−semiconductor nanocomposite systems.

■ ASSOCIATED CONTENT

Supporting Information

The Supporting Information is available free of charge on the ACS Publications website at DOI: 10.1021/acs.nanolett.5b02030.

Information on (i) synthesis of Ag nanoparticles and Ag/ZnO nanocomposites and (ii) EELS experimental details (PDF)

■ AUTHOR INFORMATION

Corresponding Authors

*E-mail: jingyue.liu@asu.edu.
*E-mail: xdbai@iphy.ac.cn.

Author Contributions

J.W. performed the STEM-EELS experiments. J.L. and J.W. designed the experiments and wrote the manuscript. J.X. synthesized the ZnO, Ag, and Ag/ZnO samples. N.J. and X.B. provided critical comments, reviewed, and revised the manuscript. All authors have read and given approval to the final version of the manuscript.

Funding

This work was funded by the start-up fund of the College of Liberal Arts and Sciences of Arizona State University and by the National 973 program (Grant Nos. 2012CB933003 and 2013CB93201) and NSF (Grant No. 11474337) of China. The authors acknowledge the use of facilities in the John M. Cowley Center for High Resolution Electron Microscopy at Arizona State University.

Notes

The authors declare no competing financial interest.

■ ABBREVIATIONS

NP, nanoparticle; NW, nanowire; LSP, localized surface plasmon; STEM-EELS, scanning transmission electron microscopy- electron energy loss spectroscopy; UP, upper branch plexciton; LP, lower branch plexciton

■ REFERENCES

(1) Mokari, T.; Rothenberg, E.; Popov, I.; Costi, R.; Banin, U. *Science* **2004**, *304*, 1787−1790.
(2) Mokari, T.; Sztrum, C. G.; Salant, A.; Rabani, E.; Banin, U. *Nat. Mater.* **2005**, *4*, 855−863.
(3) Zhang, W.; Govorov, A.; Bryant, G. *Phys. Rev. Lett.* **2006**, *97*, 146804.
(4) Costi, R.; Saunders, A. E.; Banin, U. *Angew. Chem., Int. Ed.* **2010**, *49*, 4878−4897.
(5) Manjavacas, A.; Garcia de Abajo, F. J.; Nordlander, P. *Nano Lett.* **2011**, *11*, 2318−2323.
(6) Tame, M. S.; McEnery, K. R.; Özdemir, Ş. K.; Lee, J.; Maier, S. A.; Kim, M. S. *Nat. Phys.* **2013**, *9*, 329−340.
(7) Jiang, R.; Li, B.; Fang, C.; Wang, J. *Adv. Mater.* **2014**, *26*, 5274−309.
(8) Achermann, M. *J. Phys. Chem. Lett.* **2010**, *1*, 2837−2843.
(9) Ebner, J.; Trügler, A.; Hohenester, U. *Eur. Phys. J. B* **2015**, *88*, 11−19.
(10) Climente, J. I.; Movilla, J. L.; Goldoni, G.; Planelles, J. *J. Phys. Chem. C* **2011**, *115*, 15868−15874.
(11) Lee, J.; Hernandez, P.; Lee, J.; Govorov, A. O.; Kotov, N. A. *Nat. Mater.* **2007**, *6*, 291−295.
(12) Okamoto, K.; Niki, I.; Shvartser, A.; Narukawa, Y.; Mukai, T.; Scherer, A. *Nat. Mater.* **2004**, *3*, 601−605.

DOI: 10.1021/acs.nanolett.5b02030
Nano Lett. 2015, 15, 5926−5931

(13) Luk'yanchuk, B.; Zheludev, N. I.; Maier, S. A.; Halas, N. J.; Nordlander, P.; Giessen, H.; Chong, C. T. *Nat. Mater.* **2010**, *9*, 707−715.
(14) Delga, A.; Feist, J.; Bravo-Abad, J.; Garcia-Vidal, F. J. *J. Opt.* **2014**, *16*, 114018.
(15) Chen, X.-W.; Sandoghdar, V.; Agio, M. *Phys. Rev. Lett.* **2013**, *110*, 153605.
(16) Gómez, D. E.; Roberts, A.; Davis, T. J.; Vernon, K. C. *Phys. Rev. B: Condens. Matter Mater. Phys.* **2012**, *86*, 035411.
(17) Ridolfo, A.; Di Stefano, O.; Fina, N.; Saija, R.; Savasta, S. *Phys. Rev. Lett.* **2010**, *105*, 263601.
(18) Artuso, R. D.; Bryant, G. W. *Phys. Rev. B: Condens. Matter Mater. Phys.* **2010**, *82*, 195419.
(19) Yan, J.-Y.; Zhang, W.; Duan, S.; Zhao, X.-G.; Govorov, A. *Phys. Rev. B: Condens. Matter Mater. Phys.* **2008**, *77*, 165301.
(20) Maaroof, A. I.; Lee, H.; Heo, K.; Park, J.; Cho, D.; Lee, B. Y.; Seong, M.-J.; Hong, S. *J. Phys. Chem. C* **2013**, *117*, 24543−24548.
(21) Song, J.-H.; Atay, T.; Shi, S.; Urabe, H.; Nurmikko, A. V. *Nano Lett.* **2005**, *5*, 1557−1561.
(22) Lee, J.; Govorov, A. O.; Dulka, J.; Kotov, N. A. *Nano Lett.* **2004**, *4*, 2323−2330.
(23) Govorov, A.; Lee, J.; Kotov, N. *Phys. Rev. B: Condens. Matter Mater. Phys.* **2007**, *76*, 125308.
(24) Hernández-Martínez, P.; Govorov, A. *Phys. Rev. B: Condens. Matter Mater. Phys.* **2008**, *78*, 035314.
(25) Cade, N.; Ritman-Meer, T.; Richards, D. *Phys. Rev. B: Condens. Matter Mater. Phys.* **2009**, *79*, 241404.
(26) Eizner, E.; Ellenbogen, T. *Appl. Phys. Lett.* **2014**, *104*, 223301.
(27) Lawrie, B. J.; Kim, K. W.; Norton, D. P.; Haglund, R. F., Jr. *Nano Lett.* **2012**, *12*, 6152−6157.
(28) Zheng, Y. B.; Kiraly, B.; Cheunkar, S.; Huang, T. J.; Weiss, P. S. *Nano Lett.* **2011**, *11*, 2061−2065.
(29) Fofang, N. T.; Grady, N. K.; Fan, Z.; Govorov, A. O.; Halas, N. J. *Nano Lett.* **2011**, *11*, 1556−1560.
(30) Zheng, Y. B.; Juluri, B. K.; Lin Jensen, L.; Ahmed, D.; Lu, M.; Jensen, L.; Huang, T. J. *Adv. Mater.* **2010**, *22*, 3603−3607.
(31) Sugawara, Y.; Kelf, T.; Baumberg, J.; Abdelsalam, M.; Bartlett, P. *Phys. Rev. Lett.* **2006**, *97*, 260401.
(32) Bellessa, J.; Bonnand, C.; Plenet, J.; Mugnier, J. *Phys. Rev. Lett.* **2004**, *93*, 036404.
(33) Tang, Z. K.; Wong, G. K. L.; Yu, P.; Kawasaki, M.; Ohtomo, A.; Koinuma, H.; Segawa, Y. *Appl. Phys. Lett.* **1998**, *72*, 3270.
(34) Yi, G.-C.; Wang, C.; Park, W. I. *Semicond. Sci. Technol.* **2005**, *20*, S22−S34.
(35) Klingshirn, C. *ChemPhysChem* **2007**, *8*, 782−803.
(36) Aranovich, J. *J. Vac. Sci. Technol.* **1979**, *16*, 994−1003.
(37) Yang, S.; Tian, X.; Wang, L.; Wei, J.; Qi, K.; Li, X.; Xu, Z.; Wang, W.; Zhao, J.; Bai, X.; Wang, E. *Appl. Phys. Lett.* **2014**, *105*, 071901.
(38) Pacholski, C.; Kornowski, A.; Weller, H. *Angew. Chem.* **2004**, *116*, 4878−4881.
(39) Lai, C. W.; An, J.; Ong, H. C. *Appl. Phys. Lett.* **2005**, *86*, 251105.
(40) Lei, D. Y.; Li, J.; Ong, H. C. *Appl. Phys. Lett.* **2007**, *91*, 021112.
(41) Cheng, P.; Li, D.; Yuan, Z.; Chen, P.; Yang, D. *Appl. Phys. Lett.* **2008**, *92*, 041119.
(42) Philipp, M.; Knupfer, M.; Büchner, B.; Gerardin, H. *J. Appl. Phys.* **2011**, *109*, 063710.
(43) Yin, J.; Yue, C.; Zang, Y.; Chiu, C. H.; Li, J.; Kuo, H. C.; Wu, Z.; Li, J.; Fang, Y.; Chen, C. *Nanoscale* **2013**, *5*, 4436−4442.
(44) Chen, H.-Y.; Liu, K.-W.; Jiang, M.-M.; Zhang, Z.-Z.; Xie, X.-H.; Wang, D.-K.; Liu, L.; Li, B.-H.; Zhao, D.-X.; Shan, C.-X.; Shen, D.-Z. *Appl. Phys. Lett.* **2014**, *104*, 091119.
(45) Scholl, J. A.; Koh, A. L.; Dionne, J. A. *Nature* **2012**, *483*, 421−427.
(46) Raza, S.; Stenger, N.; Kadkhodazadeh, S.; Fischer, S. V.; Kostesha, N.; Jauho, A.-P.; Burrows, A.; Wubs, M.; Mortensen, N. A. *Nanophotonics* **2013**, *2*, 131−138.
(47) Krivanek, O. L.; Lovejoy, T. C.; Dellby, N.; Aoki, T.; Carpenter, R. W.; Rez, P.; Soignard, E.; Zhu, J.; Batson, P. E.; Lagos, M. J.; Egerton, R. F.; Crozier, P. A. *Nature* **2014**, *514*, 209−212.
(48) Nelayah, J.; Kociak, M.; Stéphan, O.; García de Abajo, F. J.; Tencé, M.; Henrard, L.; Taverna, D.; Pastoriza-Santos, I.; Liz-Marzán, L. M.; Colliex, C. *Nat. Phys.* **2007**, *3*, 348−353.
(49) Koh, A. L.; Bao, K.; Khan, I.; Smith, W. E.; Kothleitner, G.; Nordlander, P.; Maier, S. A.; McComb, D. W. *ACS Nano* **2009**, *3*, 3015−3022.
(50) Raza, S.; Kadkhodazadeh, S.; Christensen, T.; Di Vece, M.; Wubs, M.; Mortensen, N. A.; Stenger, N. *arXiv* **2015**, 1505.00594.
(51) Rafferty, B.; Brown, L. M. *Phys. Rev. B: Condens. Matter Mater. Phys.* **1998**, *58*, 10326−10337.
(52) Agranovich, V. M.; Litinskaia, M.; Lidzey, D. G. *Phys. Rev. B: Condens. Matter Mater. Phys.* **2003**, *67*, 085311.
(53) Barrow, S. J.; Rossouw, D.; Funston, A. M.; Botton, G. A.; Mulvaney, P. *Nano Lett.* **2014**, *14*, 3799−3808.
(54) Nordlander, P.; Oubre, C.; Prodan, E.; Li, K.; Stockman, M. I. *Nano Lett.* **2004**, *4*, 899−903.
(55) Prodan, E.; Radloff, C.; Halas, N. J.; Nordlander, P. *Science* **2003**, *302*, 419−422.
(56) Artuso, R. D.; Bryant, G. W. *Nano Lett.* **2008**, *8*, 2106−2111.
(57) Davis, T. J.; Gómez, D. E.; Vernon, K. C. *Nano Lett.* **2010**, *10*, 2618−2625.
(58) Raza, S.; Yan, W.; Stenger, N.; Wubs, M.; Mortensen, N. A. *Opt. Express* **2013**, *21*, 27344−27355.

DOI: 10.1021/acs.nanolett.5b02030
Nano Lett. 2015, 15, 5926−5931